Multinucleon transfer in ^{48}Ti + ^{48}Ti collisions at 11.5 MeV/nucleon

Georgios Souliotis[1,*], *Stergios* Koulouris[1], *Marcia R. D.* Rodrigues[2], *Brian* Roeder[2], *Theodoros* Depastas[2], *Njeri* Edwards[3], *Justin* Mabiala[3], *Daniela* Ramirez[2], *Thomas* Settlemyre[2], and *Aldo* Bonasera[2,4]

[1]Laboratory of Physical Chemistry, Department of Chemistry, National and Kapodistrian University of Athens, Athens, Greece
[2]Cyclotron Institute, Texas A&M University, College Station, Texas, USA
[3]Physics Department, Prairie View A&M University, Prairie View, Texas, USA
[4]Laboratori Nazionali del Sud, INFN, Catania, Italy

Abstract. In this work, experimental data of projectile fragment distributions from a preliminary experimental study of the reaction of 11.5 MeV/nucleon ^{48}Ti on ^{48}Ti analyzed with the MARS recoil separator at the Cyclotron Institute of Texas A&M University are presented. Production cross sections, momentum distributions and excitation-energy distributions are extracted and compared with calculations with the Deep Inelastic Transfer (DIT) model and the Constrained Molecular Dynamics model (CoMD). Despite the limited extent of the present dataset, an overall agreement of the models with the data is found pointing at the prevailing nucleon-exchange character of the collisions at this energy.

1 Introduction

The study of neutron-rich isotopes toward the neutron-drip line is a topical theme of nuclear physics research regarding both nuclear structure and nuclear astrophysics [1]. In parallel to the standard routes to neutron-rich nuclides (that is, spallation, fission and projectile fragmentation), an efficient production approach is offered via multinucleon transfer reactions from the Coulomb barrier to the Fermi energy [2]. The present work is a continuation of our systematic studies of the mechanisms of multinucleon-transfer reactions below the Fermi energy. It comprises mass spectrometric measurements of projectile-like fragments from the reaction of a ^{48}Ti beam with a ^{48}Ti target at 11.5 MeV/nucleon performed with the MARS recoil separator at the Cyclotron Institute of Texas A&M University. The experimental data are compared with calculations employing the DIT and the CoMD models followed by GEMINI. Production cross sections, momentum and excitation-energy distributions are discussed.

The structure of the paper is as follows. In section 2, an overview of the experiment and the data analysis is presented. In section 3, the results on experimental distributions are discussed along with comparisons to theoretical calculations followed by conclusions in section 4.

2 Experimental Setup and Data Reduction

The experiment was performed at the Cyclotron Institute of Texas A&M University along the lines of our previous works [3–5]. Below we give a brief description of the experimental set-up. A ^{48}Ti^{15+} (11.5 MeV/nucleon) beam, accelerated by the K150 Cyclotron, interacted with a ^{nat}Ti target of 1.8 mg/cm^2 thickness. For simplicity, given the 72% ^{48}Ti content of ^{nat}Ti, we report the target as ^{48}Ti throughout this paper. The MARS recoil separator [6], operated in its standard mode as a radioactive-beam separator, was used to collect the projectile fragments. The ^{48}Ti beam was sent to the primary target of MARS along its optical axis and projectile fragments were collected in a square window corresponding to horizontal and vertical angles of 2.7°, thus, defining a solid angle $\Delta\Omega$ = 2.2 msr. The fragments traversed the first dispersive section of MARS and passed through slits defining a 1% magnetic rigidity acceptance. Then they continued via the second dispersive section of MARS and passed through the velocity filter defining a 10% velocity window. Finally, they traversed the third dispersive section of MARS that provides a vertical dispersion offering an A/q separation of the fragments. The fragments were collected in a (5cm×5cm) $\Delta E-E$ Si detector telescope consisting of a 68 μm resistive 16-strip detector and followed by a 1000 μm detector.

To identify the fragments and obtain the atomic number Z, mass number A, velocity and ionic charge, the following procedure was applied. First, the Si detector telescope was calibrated using the elastically scattered beam and a ^{32}S (11.5 MeV/nucleon) analog beam, present as impurity in some runs. Guided by Bethe-Bloch equation, an empirical relation of the velocity was obtained as a function of energy loss and total energy for the A/Z range of interest, expressed as:

$$\upsilon \propto \left(\frac{E_{tot}}{\sqrt{\Delta E}}\right)^{\frac{1}{3}} \quad (1)$$

where ΔE is the energy loss in the first Si detector and E_{tot} = ΔE + E_r is the sum of the energy loss ΔE and the residual energy E_r in the second Si detector.

*e-mail: soulioti@chem.uoa.gr

The atomic number of the ejectiles was reconstructed from the extracted velocity (as above) and the energy loss ΔE assuming a linear dependence with respect to $\upsilon\sqrt{\Delta E}$ as in our recent work [7, 8]. A correlation of the reconstructed atomic number Z with respect to the vertical position Y of the final focal plane is shown in the upper panel of Fig. 1. In this figure, gates (contours) have been drawn to select the respective Z of the events. Observable in this figure is the presence of the ^{32}S impurity beam at the lower right part of the spectrum. The ionic charge state of the ejectiles is obtained from the magnetic rigidity equation:

$$B\rho = \frac{p}{A}\frac{A}{q} \tag{2}$$

The magnetic rigidity is given by the setting of the spectrometer with width of 1% defined by the opening of the slits at the intermediate image, as mentioned earlier. The momentum per nucleon p/A is essentially the velocity obtained as above. Finally, for the purpose of extracting q, the mass number is obtained from the total energy and the velocity. A correlation of the Y position with respect to the reconstructed ionic charge state q is presented in the middle panel of Fig. 1. Gates (contours) are drawn to select the q of the events. Again, the ^{32}S impurity beam appears at the upper left of the figure. Finally, a correlation of the A/q of the ions with respect to the Y position was obtained assuming a linear relation of the form:

$$\frac{A}{q} = B\rho_0(\alpha_0 + \alpha_1 Y) \tag{3}$$

where $B\rho_0$ is the magnetic rigidity of a given setting of the separator. The coefficients α_0 and α_1 were determined from the position of elastically scattered projectiles at various charge states and $B\rho_0$ settings. Using the above equation along with the q determination from Eq. 2, the mass number A of the ejectiles was obtained. A correlation of A with respect to E_{tot} is shown in the last panel of Fig. 1, for Z = 23 and q = 22. For each Z and q, such A-E_{tot} plots were obtained and gates were drawn to obtain the corresponding yields.

After appropriate combination and normalization of the data using the measured beam current for the various runs, the distribution of the yield was obtained with respect to Z, A, q and p/A. The distributions were summed over the contributing q and using the beam current and target thickness, cross sections were obtained with respect to Z, A and p/A in the angular window ΔΩ = 2.2 msr and magnetic rigidity covered by the experimental settings. Summing over p/A provided the yield distributions with respect to Z and A (that we discuss later in Fig. 3). Furthermore, summing over Z provided the isobaric mass distributions that we show in Fig. 2 and discuss below.

During this experiment, data were obtained in several magnetic rigidity settings of the spectrometer in the range of 1.0-1.3 Tm. However, the settings did not correspond to overlapping magnetic rigidity windows; this resulted in large gaps in the momentum per nucleon spectra, as we will see later on. Nevertheless, we were able to account for this feature via detailed filtering of the calculations for both angular and magnetic rigidity acceptance.

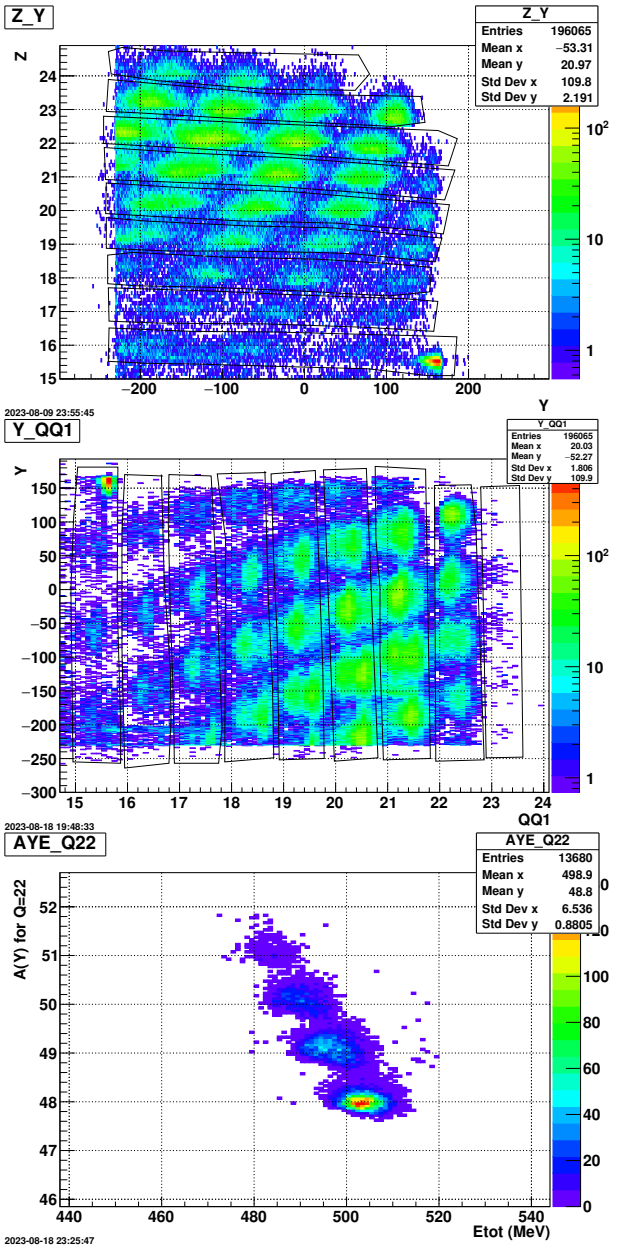

Figure 1. Representative results of the particle identification procedure. Upper panel: atomic number Z versus Y position. Middle panel: Y position versus ionic charge state q. Lower panel: mass number A versus E_{tot} for Z = 23 and Q = 22 (see text).

3 Results and Comparison with Theoretical Calculations

In this section, the experimental results of ejectile distributions from the reaction of ^{48}Ti with ^{48}Ti at 11.5 MeV/nucleon will be presented and compared with theoretical calculations. The calculations are performed using a standard two-stage Monte Carlo approach. In the first, dynamical stage, the interaction between the projectile and the target was described by the phenomenological DIT model [9] and the microscopic CoMD model [10]. After the dynamical stage, the primary fragments

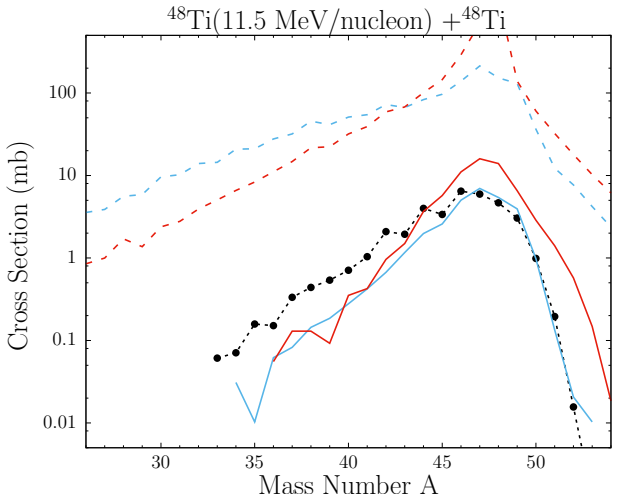

Figure 2. Isobaric mass distributions from ^{48}Ti (11.5 MeV/nucleon) + ^{48}Ti. Experimental Data: Closed (black) circles. The calculations shown are DIT by a dashed (blue) line for total nuclide cross sections and by a solid (blue) line for nuclide cross sections filtered for the angular and magnetic rigidity acceptance. The CoMD calculations share the same symbolism, but with a red color.

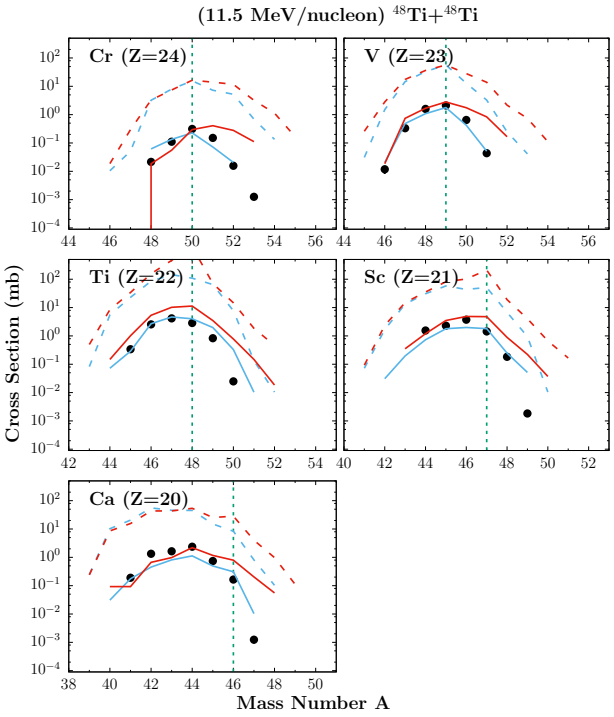

Figure 3. Production cross sections (mass distributions) of elements with Z=20-24 from ^{48}Ti (11.5 MeV/nucleon) + ^{48}Ti. Experimental Data: Closed (black) circles. The calculations shown are DIT by a dashed (blue) line for total nuclide cross sections and by a solid (blue) line for nuclide cross sections filtered for the angular and magnetic rigidity acceptance. The CoMD calculations share the same symbolism, but with a red color.

undergo de-excitation, which is modeled by the statistical de-excitation code GEMINI [11]. For the purposes of this study, the combined results from these calculations will be referred to as DIT and CoMD calculations, respectively.

3.1 Mass Distributions

Before discussing the nuclide production cross sections, we present in Fig. 2 the isobaric cross sections. The experimental data are given by the closed symbols. The dashed lines indicate the calculated total cross sections by the DIT model (blue lines) and the CoMD model (red lines). The full lines are the cross sections that result after filtering for the angular acceptance and the magnetic rigidity range covered in the experiment. It is interesting to note the good agreement of the DIT calculation with the data from mass A = 45 - 52, albeit the slight underestimation below A = 45. The CoMD calculations appear to be higher than the data above A = 45 and show a steeper slope below A = 45. Moreover, the total calculations show the same behaviour as the corresponding filtered ones. Finally, comparing the two lines of the DIT calculation (total and filtered), we observe that the angular and magnetic rigidity acceptance of this test experiment were such as to accept only 1/20 of the cross section in this forward angle (and rather small $\Delta\Omega$ acceptance) of the experimental setup. Our calculations show that complete coverage of the magnetic rigidity region of the ejectiles from this reaction (with adjacent runs in steps of 1%) would give a factor of about 4 in the yields. The remaining factor corresponds to the limited angular acceptance of the MARS separator. Consequently, a large acceptance separator would be necessary for a more efficient collection (see e.g. Ref. [8] and references therein).

In Fig. 3, we present mass distributions for the observed isotopes of the elements with Z = 20–24 from the reaction ^{48}Ti (11.5 MeV/nucleon) with ^{48}Ti. The experimental data are shown by the closed black circles. The vertical dashed (green) line indicates the initiation of neutron pickup. We note that the production of several neutron-rich nuclides corresponding to the pickup of 2 neutrons from the target has been achieved, as can be see, e.g., in the case of Sc (Z=21) isotopes. The data are also compared with the DIT and CoMD calculations, shown by the blue and red lines, respectively. The dashed lines indicate total nuclide cross sections, whereas the solid lines indicate the cross sections after filtering for the angular acceptance of MARS and the magnetic rigidity intervals covered in this experiment. We observe that the DIT calculations lead to cross sections that are in overall reasonable agreement with the experimental data (e.g. in the case of Ti and V isotopes). Regarding the CoMD calculations, we observe that they give in general an overall description of the shape of the experimental yield distributions, but they tend to overpredict the neutron-rich sides of the distributions.

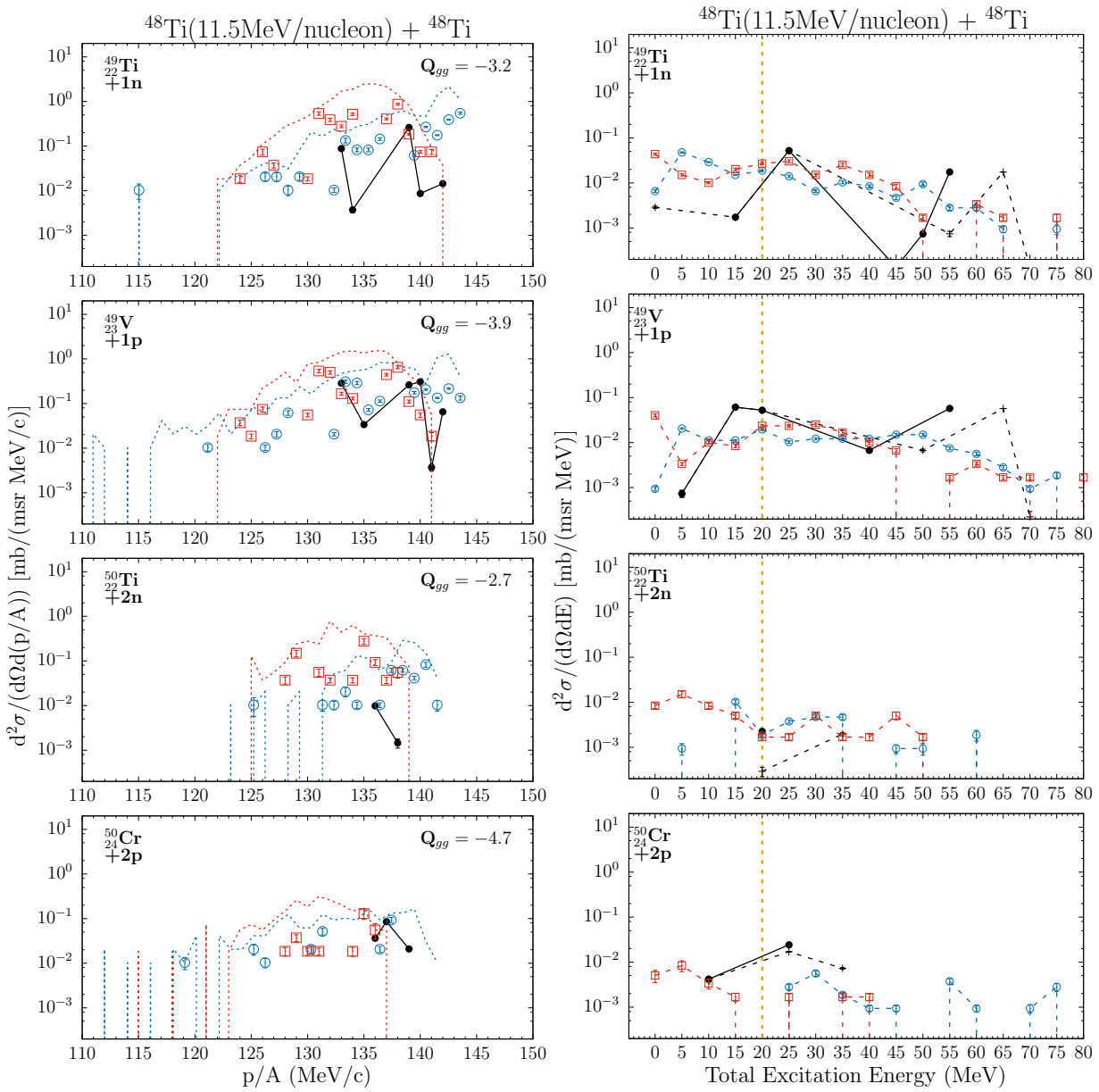

Figure 4. Left panels: Momentum per nucleon distributions of ejectiles from pickup channels of the reaction ^{48}Ti (11.5 MeV/nucleon) + ^{48}Ti. Experimental Data: closed (black) circles with full lines. Right panels: Reconstructed excitation energy distributions of ejectiles for the same channels. Experimental Data: Neutron evaporation-only [closed (black) circles with full lines], no evaporation [(black) crosses with dashed lines]. The DIT calculations [open (blue) circles] and CoMD calculations [open (red) squares] incorporate filtering for the angular acceptance and the magnetic rigidity coverage in the experiment. The dotted lines in the left panels of the figure (DIT: blue line, CoMD: red line) represent filtering for the angular acceptance only (see text).

3.2 Momentum and Excitation Energy Distributions

In this subsection, we will show momentum per nucleon distributions and reconstructed excitation energy distributions from various reaction channels. We note that the momentum per nucleon (p/A), namely the velocity, can be used as an indicator of energy dissipation. The general behaviour of the p/A distributions, as presented in previous works [5, 8] and will be seen later on, exhibit two main regions: a) a quasielastic region corresponding to direct processes, and b) a broad region at lower p/A values indicative of deep inelastic processes.

In Fig. 4, we present momentum and excitation energy distributions of various nucleon pickup channels of the reaction ^{48}Ti (11.5 MeV/nucleon) + ^{48}Ti. Specifically, we present the distributions of ejectiles with pickup of one and two neutrons, as well as the pickup of one and two protons from the target. First, we will focus on the p/A distributions which are depicted on the left panels of Fig. 4. The experimental data are shown by closed black points. The

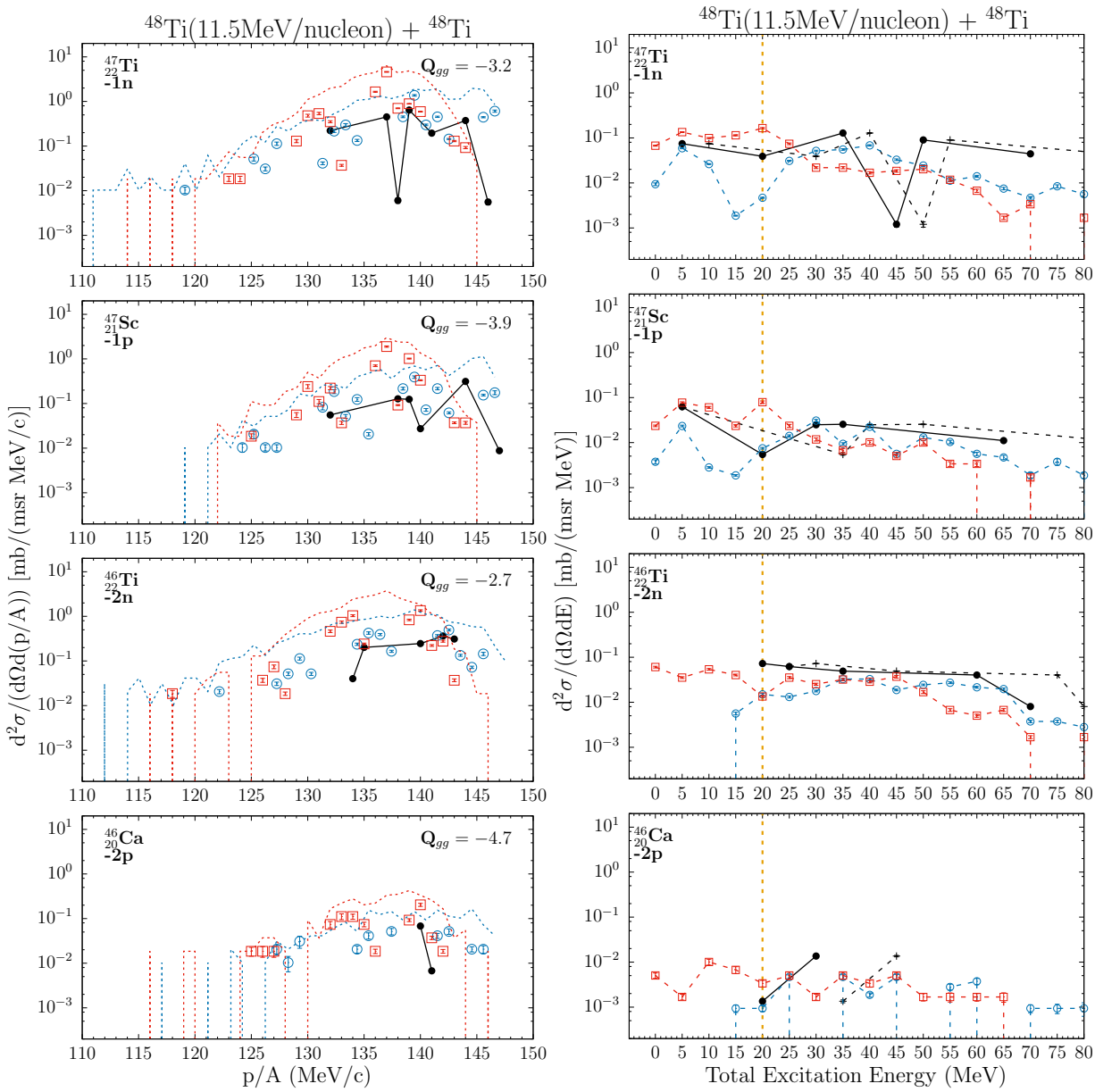

Figure 5. Left panels: Momentum per nucleon distributions of ejectiles from stripping channels of the reaction ^{48}Ti (11.5 MeV/nucleon) + ^{48}Ti. Experimental Data: closed (black) circles with full lines. Right panels: Reconstructed excitation energy distributions of ejectiles for the same channels.Experimental Data: Neutron evaporation-only [closed (black) circles with full lines], no evaporation [(black) crosses with dashed lines]. The DIT calculations [open (blue) circles] and CoMD calculations [open (red) squares] incorporate filtering for the angular acceptance and the magnetic rigidity coverage in the experiment. The dotted lines in the left panels of the figure (DIT: blue line, CoMD: red line) represent filtering for the angular acceptance only (see text).

vertical axis gives the value of the double differential cross section $\frac{d^2\sigma}{d\Omega d(P/A)}$ in units of $[\frac{mb}{msr(MeV/c)}]$. The behaviour of the experimental spectra are more or less in agreement with the general behaviour of the momentum distributions as mentioned above. The experimental data are compared with the DIT and CoMD calculations shown by blue and red colors, respectively. For each model, two calculations are shown. First, the dotted lines represent the calculations filtered for the angular acceptance of the separator, thus assuming complete coverage of the magnetic rigidity. Moreover, the open points are the calculations with the additional filtering for the exact magnetic rigidity windows covered in the experiment. We may say that, despite the limited extent of the data, the calculations, notably the DIT ones, describe the location of the data.

In the right panels of Fig. 4, we display excitation energy distributions of ejectiles for the same channels. We performed a preliminary reconstruction of the total excitation energy of the quasiprojectile (QP)-quasitarget (QT) binary system based on binary kinematics on an event-by-

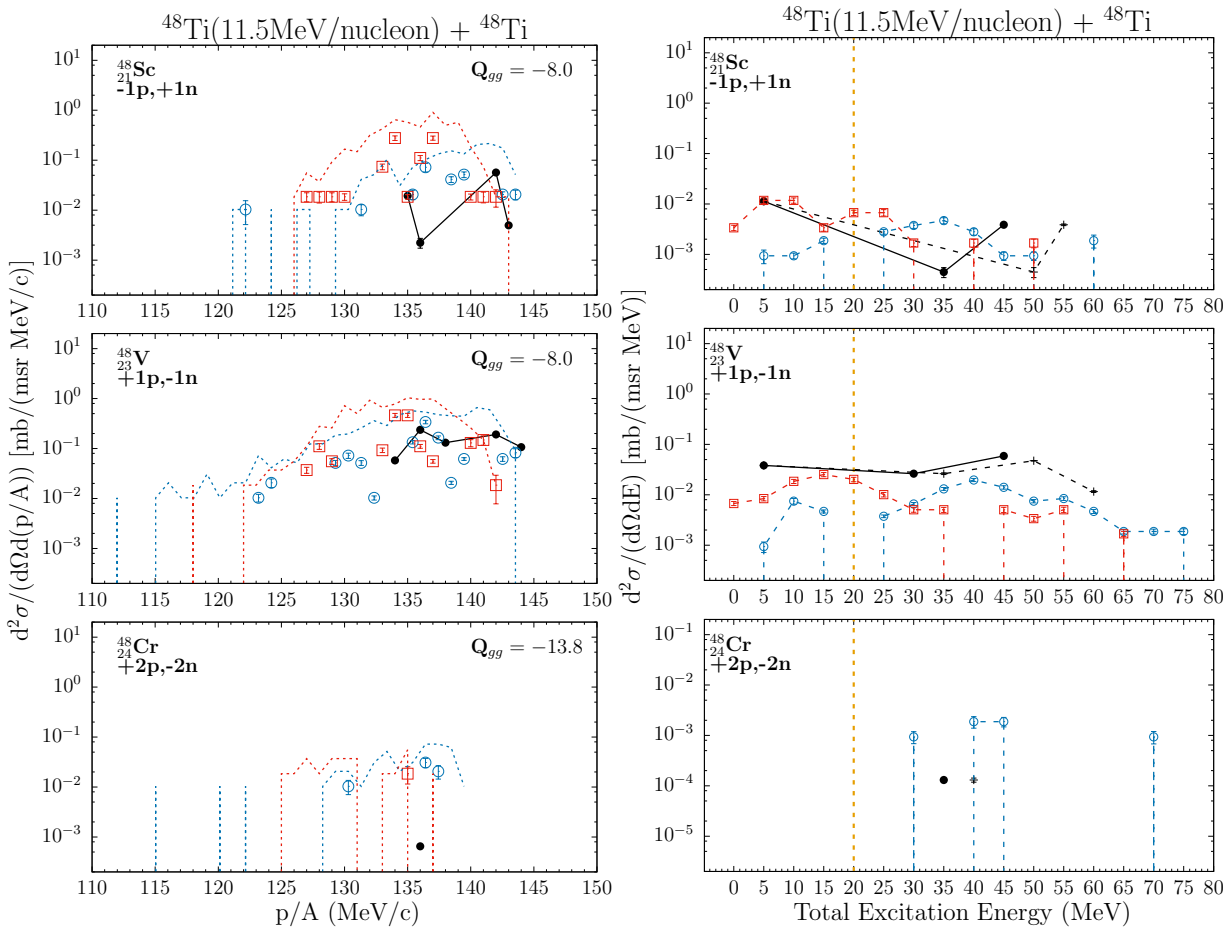

Figure 6. Left panels: Momentum per nucleon distributions of ejectiles from charge exchange channels of the reaction ^{48}Ti (11.5 MeV/nucleon) + ^{48}Ti. Experimental Data: closed (black) circles with full lines. Right panels: Reconstructed excitation energy distributions of ejectiles for the same channels. Experimental Data: Neutron evaporation-only [closed (black) circles with full lines], no evaporation [(black) crosses with dashed lines]. The DIT calculations [open (blue) circles] and CoMD calculations [open (red) squares] incorporate filtering for the angular acceptance and the magnetic rigidity coverage in the experiment. The dotted lines in the left panels of the figure (DIT: blue line, CoMD: red line) represent filtering for the angular acceptance only (see text).

event basis, following the approach outlined in Ref. [12]. The reconstruction was performed under two assumptions. The first assumption considers neutron emission only (represented by closed black circles with full lines), while the second assumes no neutron (or other particle) evaporation (depicted by black crosses with dashed lines). These experimental results are compared with DIT calculations and CoMD calculations, shown as open (blue) circles and open (red) squares, respectively. The vertical axis gives the double differential cross section $\frac{d^2\sigma}{d\Omega dE}$ in units of $[\frac{mb}{msr(MeV)}]$. The (orange) vertical dashed line at 20 MeV represents an empirical threshold of quasielastic processes defining the limit of no neutron emission from the QP. The general behaviour of the reconstructed excitation energy distributions is a rather flat shape with respect to the total excitation energy of the primary binary system. The experimental data assuming no evaporation extend to higher excitation energies than the data assuming only neutron evaporation in the dissipative region (high total excitation energy). Furthermore, the experimental data, despite their limited extent, seem to be in overall agreement with the DIT and the CoMD calculations.

In Fig. 5, we present the p/A distributions and the reconstructed excitation energy distributions of various stripping channels of the same reaction. We also note that the excitation energy distributions have a rather flat behaviour and are in fair agreement with the DIT and CoMD calculations. Finally in Fig. 6, we present the p/A distributions and excitation energy distributions of charge exchange channels of the same reaction. As before, the behaviour of the data, taking into account their limited extent, is rather flat [e.g. in the case of the (-1p,+1n) and (+1p,-1n) channels] and appear to be described by the DIT and CoMD calculations. Finally, for the (+2p,-2n) channel, we have no CoMD results due to rather limited statistics after the filtering procedure, whereas the DIT calculation describes the location of the data, albeit higher.

4 Conclusions

In this work we presented data on ejectile distributions from a test run performed with a beam of ^{48}Ti (11.5 MeV/nucleon) on a ^{48}Ti target. The ejectiles were analyzed with the MARS recoil separator operated in its "standard" operation mode as a radioactive beam separator. The production cross sections, momentum per nuleon (p/A) distributions and excitation energy distributions were compared with calculations using the DIT and the CoMD codes followed by the de-excitation code GEMINI. Furthermore, the calculations were filtered for the angular and magnetic rigidity acceptance. Despite the rather incomplete nature of the present dataset, an overall agreement of the models (especially the DIT model) is seen, suggesting that the prevailing mechanism at this energy is that of a stochastic nucleon exchange, along with the expected direct transfer at low excitation energy.

Using the methodology developed in this work, our future plan includes measurements with complete magnetic rigidity coverage, allowing to obtain high-quality data in the full excitation energy region from quasielastic to deep-inelastic processes. This will enable systematic comparisons with our data at 15 MeV/nucleon and 25 MeV/nucleon in order to study the evolution of the reaction mechanisms below the Fermi energy and the optimum conditions for producing neutron-rich nuclides.

5 Acknowledgements

We thank the cyclotron crew at Texas A&M University for the excellent beam quality. Work supported in part by the United States Department of Energy (DOE), Office of Science, Office of Nuclear Physics under grant DE-FG02-93ER40773 and the National Nuclear Security Administration, Center for Excellence in Nuclear Training and University Based Research (CENTAUR) under grant DE-NA0003841. G.S. acknowledges support from the Special Account for Research Grants of the National and Kapodistrian University of Athens.

References

[1] G. G. Adamian, N. V. Antonenko, A. Diaz-Torees, S. Heinz, How to extend the chart of nuclides? Eur. Phys. J. A **56:47** (2020). https://doi.org/10.1140/epja/s10050-020-00046-7

[2] B. Borderie, M.F. Rivet, L. Tassan-Got, Heavy-ion peripheral collisions in the Fermi energy domain. Ann. Phys. Fr., 15:4 pp. 287-390 (1990). https://doi.org/10.1051/anphys:01990001504028700

[3] G. A. Souliotis, M. Veselsky, G. Chubarian, L. Trache, A. Keksis, E. Martin, A. Ruangma, E. Winchester, S.J, Yennello, Enhanced production of neutron-rich rare isotopes in the reaction of 25 MeV/nucleon ^{86}Kr on ^{64}Ni. Phys. Lett. B **543**, 163 (2002). https://doi.org/10.1016/S0370-2693(02)02459-0

[4] G. A. Souliotis, M. Veselsky, S. Galanopoulos, M. Jandel, Z. Kohley, L. W. May, D. V. Shetty, B. C. Stein, and S. J. Yennello, Approaching neutron-rich nuclei toward the r-process path in peripheral heavy-ion collisions at 15 MeV/nucleon. Phys. Rev. C **84**, 064607 (2011). https://doi.org/10.1103/PhysRevC.84.064607

[5] K. Palli, G. A. Souliotis, I. Dimitropoulos, T. Depastas, O. Fasoula, S. Koulouris, M. Veselsky, S. J. Yennello, and A. Bonasera, Microscopic description of multinucleon transfer in ^{40}Ar + ^{64}Ni collisions at 15 MeV/nucleon. EPJ Web Conf. **252**, 07002 (2021). https://doi.org/10.1051/epjconf/202125207002

[6] R. E. Tribble, R. H. Burch and C. A. Gagliardi, MARS: A momentum achromat recoil spectrometer, Nucl. Instrum. Methods A **285**, 441 (1989). https://doi.org/10.1016/0168-9002(89)90215-5

[7] G. A. Souliotis, S. Koulouris, F. Cappuzzello, D. Carbone, A. Pakou, C. Agodi et al., Identification of medium mass (A=60-80) ejectiles from 15 MeV/nucleon peripheral heavy-ion collisions with the MAGNEX large-acceptance spectrometer. Nucl. Instrum. Methods A **1031**, 166588 (2022). https://doi.org/10.1016/j.nima.2022.166588

[8] S. Koulouris, G. A. Souliotis, F. Cappuzzello, D. Carbone, A. Pakou, C. Agodi et al., Multinucleon transfer channels from ^{70}Zn (15 MeV/nucleon) + ^{64}Ni collisions. Phys. Rev. C **108**, 044612 (2023). https://doi.org/10.1103/PhysRevC.108.044612

[9] L. Tassan-Got and C. Stephan, Deep inelastic transfers: a way to dissipate energy and angular momentum for reactions in the Fermi energy domain. Nucl. Phys. A **524**, 121 (1991). https://doi.org/10.1016/0375-9474(91)90019-3

[10] M. Papa, T. Maruyama, A. Bonasera, Constraint molecular dynamics approach to fermionic systems. Phys. Rev. C **64**, 024612 (2001). https://doi.org/10.1103/PhysRevC.64.024612

[11] R. J. Charity, M. A. McMahan, G. J. Wozniak, R. J. McDonald, L. G. Moretto, D. G. Sarantites et al., Systematics of complex fragment emission in niobium-induced reactions. Nucl. Phys. A **483**, 371 (1988). https://doi.org/10.1016/0375-9474(88)90542-8

[12] G. A. Souliotis, P. N. Fountas, M. Veselsky, S. Galanopoulos, Z. Kohley, A. McIntosh, S. J. Yennello, and A. Bonasera, Isoscaling of heavy projectile residues and N/Z equilibration in peripheral heavy-ion collisions below the Fermi energy. Phys. Rev. C **90**, 064612 (2014). https://doi.org/10.1103/PhysRevC.90.064612